INORGANIC CHEMISTRY FRONTIERS

RESEARCH ARTICLE

View Article Online
View Journal

Cite this: DOI: 10.1039/d6qi00025h

Stable nickel complexes of a siliconoid/silylene hybrid ligand: competent hydrosilylation catalysts for terminal olefins

Luisa Giarrana,[a] Dennis Welterlich,[a] Michael Zimmer,[a] Bernd Morgenstern[b] and David Scheschkewitz *[a]

Received 5th January 2026,
Accepted 11th February 2026

DOI: 10.1039/d6qi00025h

rsc.li/frontiers-inorganic

The use of abundant, first row transition metals instead of platinum group metals is a contemporary goal in homogenous catalysis research. Electron-rich silylenes are increasingly established as viable alternatives to carbene-based ligand systems. Here we report that – depending on the first row transition metal fragment employed – a silylene hybridized with a Si_7-siliconoid (Tip_5Si_7NHSi **1**) either coordinates to the metal centre *via* the silylene side-arm exclusively ($Fe(CO)_4$ complex) and thus retains an unperturbed metalloid core or coordinates in a chelating manner involving the donation by unsubstituted vertices (Ni(cod)-fragment, cod = 1,5-cyclooctadiene). The siliconoid/silylene ligand **1** is bonded more strongly than cod so that the latter is readily replaced by PPh_3 or CO ligands. The cod derivative is catalytically active in the hydrosilylation of terminal olefins with the secondary silane Ph_2SiH_2.

Introduction

Transition metal complexes are still the benchmark in homogenous catalysis. Especially the precious late 4d and 5d transition metals show outstanding catalytic activity in the value-added transformations of small molecules such as CO, CO_2, NH_3 or H_2.[1,2] The toxicity, low abundance and high price of these metals moved 3d transition metals into focus over the last years.[3] Their lower propensity for $2e^-$ redox steps, however, requires the use of non-innocent ligands and hence metal–ligand cooperativity in many cases.[4,5] More recently, the incorporation of heavier elements of the p-block into the ligand system has proven to induce chemical non-innocence.[6–10] In particular, low-valent motifs such as silylenes, germylenes and stannylenes have been employed as ligands towards base metals in order to improve their performance in homogenous catalysis.[11–19]

Even with chemically innocent coordination environment, nickel is an outstanding catalyst in many homogenous transformations, for instance, in alkene hydrogenation and cross-coupling reactions.[20,21] The nickel complexes with amidinato-stabilized silicon(II) **I**[22] and with dialkylsilylene ligand **II** (Fig. 1)[23] paved the way for a broad variety of stable Ni(0) complexes with low-valent group 14 ligands.[11,24–28] A mixed NHC/NHSi-stabilized Ni complex **III** reported by Driess *et al.* activates dihydrogen and thus reductively transforms HBcat into a Ni^{II} borylene complex.[24] Subsequently, various bis(silylenes) with different bridging backbones such as **IV**,[25] **V**[26] or **VI**[27]

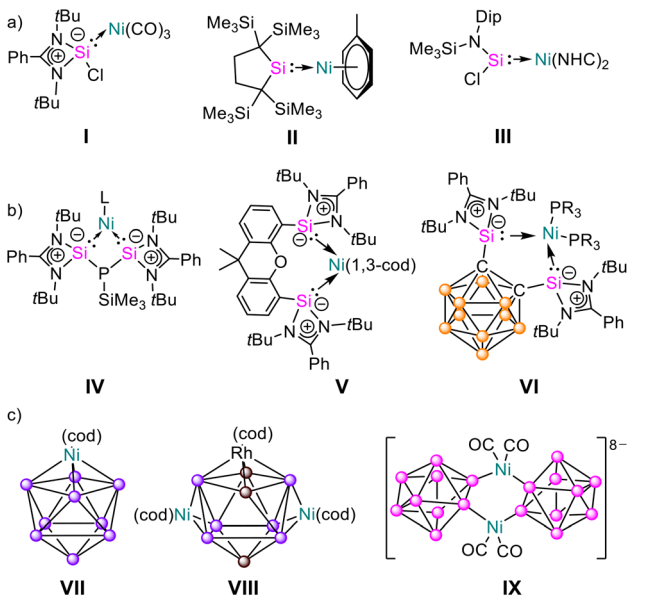

Fig. 1 Selected examples of low-valent group 14 ligands with nickel (a, b and c) (○ = BH, ○ = Ge, ○ = Ge-Hyp (Hyp = $Si(SiMe_3)_3$), ○ = Si, Dip = 2,6-diisopropylphenyl, 1,3-cod = 1,3-cyclooctadienyl, cod = 1,5-cyclooctadienyl, NHC = *N*,*N*′-diisopropyl-3,4-dimethylimidazol-2-ylidene).

[a]*Krupp-Chair for General and Inorganic Chemistry, Saarland University, 66123 Saarbrücken, Germany. E-mail: scheschkewitz@mx.uni-saarland.de*
[b]*Service Center X-ray Diffraction, Saarland University, 66123 Saarbrücken, Germany*

were employed as bidentate ligands for nickel to result in the activation of H_2, CO, or NH_3 and other small molecules.[11–19,28]

Group 14-based cluster systems[29–31] have recently come to the fore as potentially redox-active ligands, but examples of their coordination to nickel are scarce and studies on catalytic activity even rarer. The Goicoechea group reported on the capping of a Ni(II) centre onto the dianionic Ge_9 Zintl cluster **VII**[32] (Fig. 1). The corresponding rhodium derivative can be converted to the heterodimetallic Ni_2-Rh-Ge_9 cluster **VIII**.[33] Although the Rh-Ge_9-cluster is an active catalyst in the hydrogenation of cyclooctadiene (cod), in case of **VII** no information on catalytic activity is available. The only silicon-cluster based nickel complex thus far was isolated by Korber *et al.* as the eightfold negative charged, dimeric Si_9–$(Ni(CO)_2)_2$–Si_9 cluster **IX**[34] with no reported catalytic activity. Siliconoids (unsaturated silicon clusters)[29,30,35–40] have been employed as ligands to various transition metals.[36,37] The incorporation of an amidinato silicon(II) side arm proved a useful strategy to enable coordination to electroneutral transition metal fragments, for instance to $Fe(CO)_4$ with Si_6 siliconoid/silylene hybrid ligand **X**,[36] yet nickel complexes of siliconoids remain elusive.

In view of the catalytic activity of an iridium complex derived from **X** in alkene isomerization,[37] we had previously attempted to coordinate it to a nickel carbonyl fragment (*in situ*-generated from $Ni(cod)_2$ under CO atmosphere) but isolated nickel-free **XI** instead (Scheme 1) as the product of complete CO cleavage. DFT calculations regarding the mechanism of CO splitting, however, suggested cooperativity between the siliconoid core and the nickel centre in experimentally undetected intermediates.[38] Plausibly, the lack of space at the Si_6 core of **X** prevents the observation, let alone isolation of any involved nickel complex.

We therefore anticipated that an expansion to a Si_7 core could increase the available space for metal coordination. Indeed, we now report the isolation and full characterization of siliconoid-transition metal complexes employing a core-expanded Si_7 cluster with pending amidinato-silylene as a ligand.[40] While the $Fe(CO)_4$ fragment is only coordinated by the silylene sidearm, the reaction with $Ni(cod)_2$ results in a product with distinct interactions of the Si_7 core with the nickel centre. Straightforward ligand exchange of cod yields the corresponding PPh_3 and CO complexes. Competent catalytic activity in hydrosilylation of terminal alkenes is demonstrated. During benchmark reactions with $Ni(cod)_2$, we unexpectedly found that this simple Ni(0) precursor exhibits remarkable activity in these alkene hydrosilylations as well, which once more illustrates the importance of appropriate control experiments in homogenous catalysis.

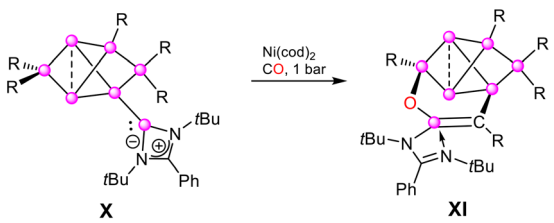

Scheme 1 Reported reaction of Si_6 siliconoid/silylene hybrid with CO in the presence of $Ni(cod)_2$ (○ = Si, R = 2,4,6-triisopropylphenyl).[38]

Results and discussion

In order to quantify our assumption regarding the reduced steric demand of the Si_7 system, we initially investigated the complexation of the Si_7 siliconoid/silylene hybrid **1**[40] to an $Fe(CO)_4$ fragment, aiming for a direct comparison with the Si_6 system **X**-$Fe(CO)_4$.[36] Reaction of **1** with one equivalent of $Fe_2(CO)_9$ at 60 °C (aluminium heating block temperature) in benzene overnight indeed leads to quantitative conversion. The desired iron tetracarbonyl complex **2** crystallizes in 46% yield from pentane (Fig. 2, top). Notably, the corresponding products could not be obtained with the corresponding germylene or stannylene-Si_7-hybrids.[40]

The molecular structure of **2** in the solid state as determined by single crystal X-ray diffraction (Fig. 2, bottom)

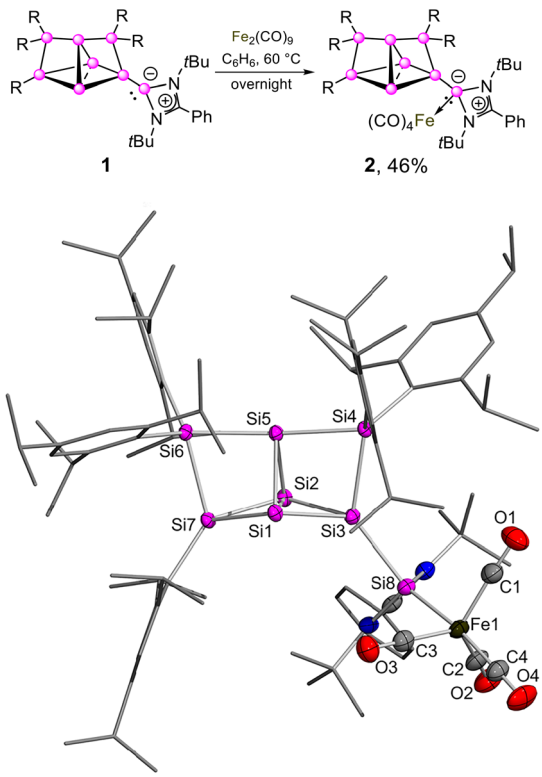

Fig. 2 Top: Reactivity of Tip_5Si_7NHSi **1** towards $Fe_2(CO)_9$ (○ = Si, R = 2,4,6-triisopropylphenyl). Bottom: Molecular structure of iron tetracarbonyl siliconoid/silylene hybrid **2** in the solid state. Hydrogen atoms are omitted for clarity. Thermal ellipsoids at 50% probability. Selected bond lengths [Å] and angles [°]: Fe–Si8 2.253(6), Si3–Si8 2.391(8), Si1–Si2 2.618(8), Si1–Si3 2.315(8), Si1–Si5 2.332(8), Si1–Si7 2.323(7), Si2–Si3 2.366(7), Si2–Si5 2.346(8), Si2–Si7 2.356(8), Si3–Si42.428(8) , Si4–Si5 2.388(7), Si5–Si6 2.381(7); Fe1–Si8–Si3 129.0(3), Si4–Si5–Si6 171.0(3), Si8–Fe1–C4 171.7(9).

reveals a silylene-coordinated Fe1 centre with a Fe–Si8 bond length of 2.253(6) Å, considerably shortened compared to **X**-Fe(CO)$_4$ (2.384 Å)[37] but well within the range of reported sterically unencumbered Si–Fe(CO)$_4$ species (2.196–2.405 Å).[41–44] The short Fe–Si bond length is a first indication for the validity of our working hypothesis that the expanded cluster core may ease the steric strain in the envisaged complexes. For a more quantitative description, we calculated the percent buried volume %V_{bur} [45,46] of **2** *vs.* that of **X**-Fe(CO)$_4$ using the SambVca open-source application.[47] As expected, **X** shows a somewhat larger buried volume of 64.9%V_{bur} in comparison with **1** (55.3%V_{bur}) at the iron centre of the Fe(CO)$_4$ fragment.[36] The assumption of a better accessibility of **1** compared to **X** is thus confirmed in principle; both values are at the upper end of the range found for typical bulky ligands. For context, common ligands for transition metals exhibit %V_{bur} values of around 30–60%.[48] Sterically more demanding ligands exceed these values: the carbazole ligand by Hinz with 74.8%,[49] the triazene by Masuda (80.1%)[50] or a tetradentate combination of N,N and P,P ligands by Constable and Housecroft (88.0%).[51]

As in **X**-Fe(CO)$_4$,[36] the Si$_7$ system **2** shows no interactions between the cluster core and the iron moiety. The Si1–Si2 distance is at 2.618(8) Å almost identical with that in the free ligand **1** (2.620 Å).[40] The CO ligands complete the trigonal–bipyramidal coordination sphere of the iron centre with C–O bond lengths (1.144–1.152 Å) and Fe1–C distances (1.769–1.794 Å) in the range of reported Fe(CO)$_4$ complexes.[41–44,52] The most notable distortion from the cluster bonding situation in the free ligand **1** is the Si4–Si5–Si6 seesaw angle of 171.0(3)° in **2**, which is slightly smaller than in **1** (174.8°).[40]

The ^{29}Si NMR spectrum of **2** shows the familiar wide signal distribution of siliconoids with eight signals in the range of 172.7 to −209.0 ppm. The signal at 172.7 ppm, assigned to Si3 based on ^{1}H/^{29}Si 2D NMR spectra, is significantly upfield-shifted compared to the free ligand **1** (211.7 ppm).[40] In contrast, the signal of the silylene moiety (Si8) is strongly downfield-shifted from 24.1 ppm (**1**)[40] to 100.5 ppm (**2**), which is very similar to the reported shift differences between **X** and its iron complex.[36] Owing to Berry pseudorotation, the ^{13}C NMR spectrum of **2** reveals only one single signal for the four characteristic CO ligands at high field at 216.79 ppm.[53]

FT-IR spectroscopy reveals four CO stretching vibrations ($\tilde{V}_{CO,exp}$ = 2026, 1953, 1923, 1907 cm^{-1}), in line with the absence of symmetry in **2**. The carbonyl stretching frequency at $\tilde{V}_{CO,exp}$ = 2026 cm^{-1} is in accordance with that of the silylene complex of Fe(CO)$_4$ ($\tilde{V}_{CO,exp}$ = 2026 cm^{-1}) reported by Jana and Roesky,[41] suggesting a similar ligand-to-metal σ-donation but a slightly higher donation than in the Si$_6$-analogue ($\tilde{V}_{CO,exp}$ = 2022 cm^{-1}). Theoretical support is provided by calculations at the B3LYP/def2-TZVPP[54–57] level of theory with stretching frequencies at $\tilde{V}_{CO,calc}$ = 2009 and 1901 cm^{-1}. The longest wavelength UV-Vis absorption of **2** occurs at $\lambda_{max,exp}$ = 525 nm (ε = 380 M^{-1} cm^{-1}) with a bathochromic shift compared to that of the Si$_6$-analogue ($\lambda_{max,exp}$ = 470 nm, ε = 1890 M^{-1} cm^{-1})[36] but a marginally hypsochromic shift compared to the starting material **1** ($\lambda_{max,exp}$ = 532 nm, ε = 704 M^{-1} cm^{-1}).[40] The experimental values for **2** are in good agreement with the TD-DFT results ($\lambda_{max,calc}$ = 528 nm; see SI for details).

For the envisaged coordination to a nickel centre, we opted for bis(cyclooctadiene) nickel(0) Ni(cod)$_2$ as precursor, given that Ni(CO)$_4$ is highly volatile and toxic (and not commercially available). Addition of 1 eq. of solid Ni(cod)$_2$ to a solution of **1** in toluene at ambient temperature caused a colour change of the mixture from brown to blackberry red. After work-up (see SI), the desired Ni-siliconoid complex **3a** was isolated as dark red, block-shaped crystals in 46% yield (Scheme 2). The residual cod ligand in **3a** can be readily replaced by adding 1 eq. of solid PPh$_3$ to the reaction mixture of **1** and Ni(cod)$_2$ affording the triphenylphosphine-derivative **3b** in 49% yield.

Single crystals were obtained from a concentrated pentane solution of **3a,b** at −26 °C. X-ray diffraction analysis confirmed the solid-state structure of **3a** in the triclinic space group $P\bar{1}$ and **3b** in the monoclinic space group $I2/a$ (Fig. 3). In contrast to the previously discussed iron complex **2**, an interaction of the transition metal atom with the Si1 and Si3 atom is observed for **3a**/**3b**. The overall decreased congestion at the unsubstituted silicon vertices given their increased number in the Si$_7$/silylene scaffold **1** compared to the Si$_6$-hybrid **X** not only allows stable nickel coordination in the first place but also gives rise to significant interactions with the cluster core. In **3a**,**b**, the Ni1 atom is not only coordinated by the central Si8 atom of the silylene unit (Si3–Si8 **3a:** 2.183(8) Å/**3b:** 2.212(5) Å), as in the case for iron in **2**, but also by the Si1 and Si3 atoms. With bond distances of 2.302(5) Å (**3a**)/2.216(8) Å (**3b**) the Si1–Ni1 bond lengths are well within the common range (2.075–2.499 Å),[19,22–28,34,58–61] while the distances between Si3 and Ni1 are with 2.428(5) Å (**3a**)/2.379(8) Å (**3b**) slightly elongated. In **3a**, a longer Si1–Ni1 bond accompanied by a shorter Si1–Si3 bond (2.429(6) Å) is observed while the reduced donor strength of PPh$_3$ leads to a contraction of the Si1–Ni1 bond and thus a slight elongation of the Si1–Si3 bond in **3b** (**3a:** 2.429(6) Å; **3b:** 2.468(1) Å). These structural parameters reflect the stronger σ-donor character of the cod ligand com-

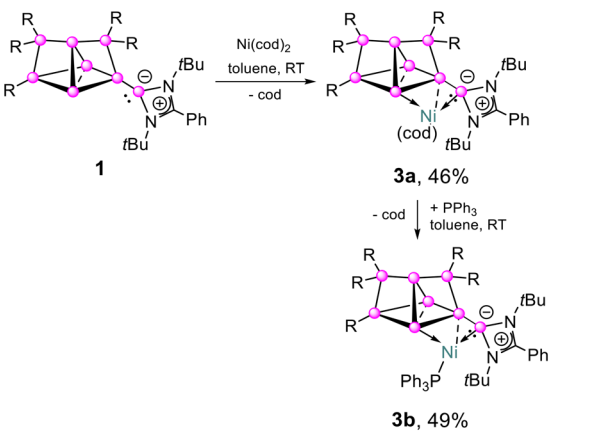

Scheme 2 Synthesis of nickel siliconoid/silylene complexes **3a** and **3b** (○ = Si, R = 2,4,6-triisopropylphenyl).

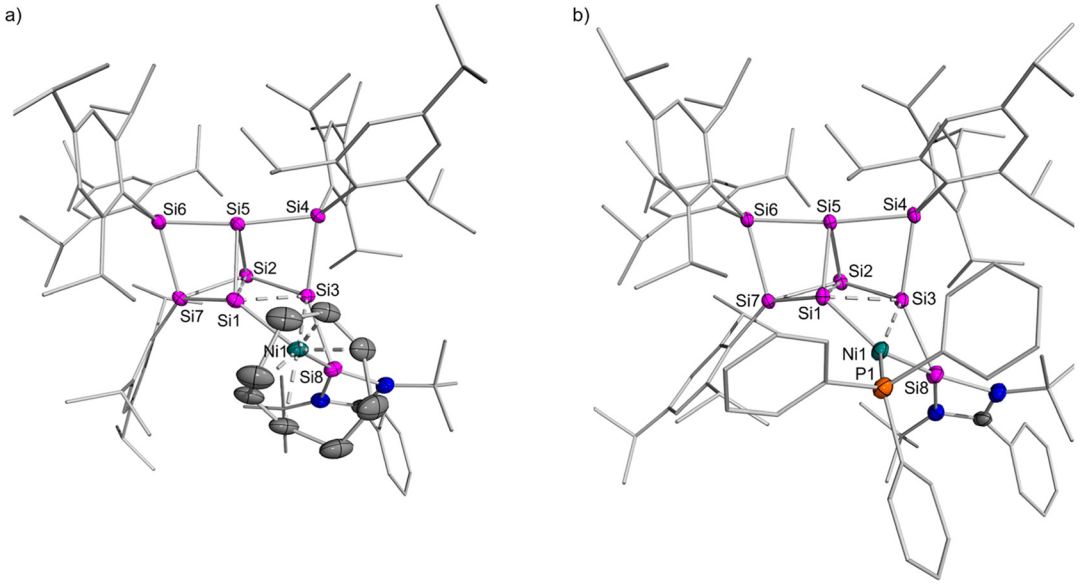

Fig. 3 Molecular structure of Ni(cod)-**3a** (left) and Ni(PPh_3)-siliconoid/silylene complex **3b** (right) in the solid state. Hydrogen atoms are omitted for clarity. Thermal ellipsoids at 50% probability. Selected bond lengths [Å] and angles [°]: (a) Ni1–Si1 2.302(5), Ni1–Si3 2.428(5), Ni1–Si8 2.212(5), Si1–Si2 2.674(6), Si1–Si3 2.429(6), Si1–Si5 2.362(6), Si1–Si7 2.324(6), Si2–Si5 2.335(6), Si2–Si7 2.352(6), Si2–Si3 2.392(1), Si3–Si8 2.291(6), Si3–Si4 2.424(6), Si4–Si5 2.371(6), Si5–Si6 2.362(6), Si6–Si7 2.425(6); Si8–Ni1–Si1 108.6(2), Si1–Ni1–Si3 61.7(2), Si8–Ni1–Si3 59.0(2), Si4–Si5–Si6 171.7(2); (b) Ni1–P1 2.200(7), Ni1–Si1 2.216(8), Ni1–Si3 2.378(8), Ni1–Si8 2.183(8), Si1–Si2 2.782(1), Si1–Si3 2.468(1), Si1–Si5 2.366(1), Si1–Si7 2.294(1), Si2–Si5 2.336(1), Si2–Si7 2.384(1), Si2–Si3 2.400(1), Si3–Si8 2.293(1), Si3–Si4 2.422(1), Si4–Si5 2.373(9), Si5–Si62.378(1), Si6–Si7 2.409(1); Si8–Ni1–Si1 120.2(3), Si1–Ni1–Si3 64.9(3), Si8–Ni1–Si3 60.2(3), Si4–Si5–Si6 173.1(4).

pared to PPh_3, while also highlighting the influence of the appreciable π-acceptor ability of PPh_3 on the electronic structure at the nickel centre. In agreement with lowered electron density in the Si_7 scaffold due to tighter bonding of the Ni1 centre in **3b** compared to **3a**, the distance between the Si1 and Si2 atom of 2.782 (1) Å in **3b** exceeds the distances between the unsubstituted vertices of so far reported propellane-like siliconoids (2.551 to 2.728 Å), while for **3a** it is with 2.674(6) Å in the reported range.[29,30,34–40] The concomitant upfield-shift of the Si2 atom in the ^{29}Si NMR spectrum of **3b** (**3a:** −340.7, **3b:** −287.6 ppm) is in line with the above mentioned shift of cluster electron density towards the perimeter of the Si2 atom. The seesaw Si4–Si5–Si6 angle in **3a** of 171.74(2)° is similar to that in **2** (171.0(3)°) and hence, slightly smaller than for **3b** (173.10(4)°) and the previously reported Si_7 cluster scaffolds ($Si_7Tip_5Cp^*$: 173.8°, Si_7Tip_5Li: 174.0°, Tip_5Si_7NHSi **1:** 174.8°).[39,40] The geometry around the Ni centre in **3a** is approximately tetrahedral with the coordinating silicon vertices (Si1 and Si8) and the two geometrical centres of the η^2-coordinated C=C double bonds of the cod ligand, which is comparable to the case of NHSi(Cl)–Ni$(CO)_3$ **I**.[22] In stark contrast, the substitution of the cod ligand by PPh_3 leads to a trigonal planar coordination environment around Ni1 in **3b** (largest deviation from Si1–Si8–Ni1–P1 plane for Ni1 = −0.018 Å), similar to the situation in **V**.[26]

Interestingly, in case of **V**, a substitution of the cod moiety by two PMe_3 units was shown to lead to a more symmetric tetrahedral geometry, a scenario likely prevented in case of **3b** by insufficient space to accommodate two PPh_3 ligands. Although the smaller $\%V_{bur}$[45,46] of **1** compared to **X** in the context of Fe$(CO)_4$ coordination indicates better accessibility as noted above, the tighter coordination under participation of the siliconoid core results in a much higher value of $\%V_{bur}$ = 69.9 at the nickel centre in **3b**.

The ^{29}Si NMR spectra of **3a** and **3b** retain the typical wide distribution observed for siliconoids,[29,30,36–40] albeit less pronounced than in **2**. The range of the chemical shifts covered in **3b** is with $\Delta\delta$ = 360.8 ppm considerably smaller in comparison to **1** but also to **3a** (Table 1), (**1**: $\Delta\delta$ = 430.7;[40] **3a** $\Delta\delta$ = 429.8 ppm). The former low-field signal of the SiTip group Si7 (**1:** 211.7 ppm, **2:** 172.7 ppm) is upfield-shifted by no less than $\Delta\delta \geq 122$ ppm for **3a** (δ = 50.0 ppm) and **3b** (δ = 63.9 ppm, d, $^4J_{P,Si}$ = 8.80 Hz). We suggest that this pronounced shielding of Si7 is a consequence of the perturbation of the cluster current,

Table 1 Experimental and calculated ^{29}Si NMR shifts (ppm) of siliconoid complexes **3a–c** at ambient temperature in C_6D_6. Calculated shifts at the TPSSh-D3(BJ)/def2-TVP[56,57,62,63] level of theory in brackets

	3a (L = cod)	**3b** (L = PPh_3)	**3c** (L = $(CO)_2$)
Si1	−154.0 [−148.1]	−87.3 (d) [−68.5]	−160.5 [−160.9]
Si2	−340.7 [−354.9]	−287.6 (d) [−291.0]	−342.2 [−354.4]
Si3	−10.2 [−9.0]	0.4 [−6.5]	−4.0 [−7.7]
Si4	−13.3 [−18.7]	−41.4 [−45.2]	−10.1 [−11.6]
Si5	−83.1 [−81.1]	−60.0 (d) [−68.2]	−81.9 [−78.5]
Si6	39.0 [35.1]	39.7 [30.6]	44.6 [37.1]
Si7	50.0 [56.5]	63.9 [65.4]	70.9 [80.1]
Si8	89.1 [90.4]	73.5 [84.6]	96.5 [93.1]

characteristic of siliconoids,[29,30,36–40] by coordination of Ni to the Si_7 core. The basal unsubstituted vertex without nickel contact Si2 is strongly shielded in both **3a** and **3b** compared to the free ligand (**3a**: −341 ppm; **3b**: −287.6 ppm (d, $^3J_{P,Si}$ = 28.5 Hz); *cf.* **1**: −219 ppm). The most downfield-shifted signals are now due to the amidinato-substituted silicon(II) centre Si1 coordinated to nickel (**3a**: 89.1 ppm; **3b**: 73.6 ppm, *cf.* **1**: 24.1 ppm (ref. 40)). The apical, substituent-free cluster vertex Si5 resonates at comparatively lower field (**3a**: −154.0 ppm; **3b**: −87.3 (d, $^3J_{P,Si}$ = 8.50 Hz) ppm; *cf.* **1**: −211.6 ppm). The $^{31}P\{^1H\}$ NMR spectrum of **3b** shows a single signal at −26.4 ppm. The shifts are in good agreement with the GIAO calculated values for the optimized structures **3a** and **3b** (B3LYP-D3(BJ)/def2-TZVP level of theory[54–57,62]) at TPSSh/def2-TZVP level of theory (Table 1).[62,63]

In case of the siliconoid/silylene hybrid ligand **X** with the Si_6 core, the addition of $Ni(cod)_2$ in a CO atmosphere had been shown to give rise to the incorporation of a completely cleaved CO moiety into the periphery of the cluster scaffold. This led to the formation of a formal Si=C double bond to the amidinato-substituted silicon(II) centre in **XI** (Scheme 1).[38] We therefore probed the behaviour of **3a,b** towards carbon monoxide. Stirring of **3a,b** under CO (1 bar) led to a colour change from blackberry red to blood red (Scheme 3). To avoid secondary decomposition reactions, the reaction was stopped immediately after disappearance of the last violet tint by removal of all volatiles under reduced pressure. The product **3c** crystallizes from pentane in 44% yield. Due to the facile decomposition in reaction mixtures and under reduced pressure, the complete work-up needed to be carried out at slightly reduced temperatures (<10 °C) until isolation of **3c** in the form of a crystalline solid, which is then stable even when redissolved.

The ^{13}C NMR spectrum of isolated **3c** shows two additional signals at low field, δ = 196.3 and 204.9 ppm, which are assigned to the carbonyl ligands based on their similarity with those of comparable Ni-carbonyl complexes (δ = 199.3 and 202.5 ppm for Roesky's amidinato silylene-$Ni(CO)_3$ **I** [22] and δ = 198.8 and 206.2 ppm for the mixed silylene–carbene coordinated $Ni(CO)_2$ complex reported by Driess[64]). The ^{29}Si NMR signals of isolated **3c** are similar to the Ni(cod) complex **3a**: a lowfield signal at 96.6 ppm for the remote silicon atom and three highfield signals at −81.9, −160.4 and −342.0 ppm for the unsubstituted Si atoms. This supports a structurally and electronically similar geometry to that of **3a**.

The longest wavelength absorption in the UV-Vis spectrum of **3a** at $\lambda_{max,exp}$ = 538 nm (ε= 8190 M^{-1} cm^{-1}) is reproduced well by TD-DFT calculations on the optimised minimum structure of **3a**. It is assigned to a combination of three transitions at $\lambda_{max,calc}$ = 546 nm (HOMO → LUMO 52.6%), 520 nm (HOMO−1 → LUMO 72.6%) and 516 nm (HOMO → LUMO+1 65.4%) at the TPSSh/def2-TZVP level of theory[56,57,62,63] (for details see SI). The different coordination geometry of the central nickel atom in **3b** is manifest in a strong red-shift of the experimental longest wavelength UV-Vis absorption of approximately $\Delta\lambda$ = 56 nm. It is observed as a broad band at $\lambda_{max,exp}$ = 596 nm (624 M^{-1} cm^{-1}) tailing to about 700 nm. Notably, the extinction coefficient is one order of magnitude smaller than in case of **3a**, which suggests considerable effect of the ligand exchange on the electronic structure (*vide infra*).

TD-DFT calculations at the TPSSh/def2-TZVP level of theory assign the observed bands to a weak transition at $\lambda_{max,calc}$ = 740 nm (HOMO → LUMO 89.6%) and slightly stronger transitions at $\lambda_{max,calc}$ = 572 nm (HOMO → LUMO+1 76.8%) and 555 nm (HOMO → LUMO+2 92.3%). A second absorption in the experimental UV-Vis spectrum of **3b** at $\lambda_{max,exp}$ = 519 nm (ε = 1127 M^{-1} cm^{-1}) is assigned to the calculated transition at 472 nm for the (HOMO−4 → LUMO 31.0%). The colour change in the reaction to **3c** to a lighter red becomes apparent in the blue-shifted absorption in the UV-Vis spectrum ($\lambda_{max,exp}$ = 525 nm, ε = 9630 M^{-1} cm^{-1}), compared to the precursors **3a** and **3b** (**3a**: $\lambda_{max,exp}$ = 538 nm, ε = 8190 M^{-} cm^{-1}, **3b**: $\lambda_{max,exp}$ = 596 nm, ε = 624 M^{-1} cm^{-1}), but in reasonable agreement with the calculated value at $\lambda_{max,calc}$ = 506 nm, (HOMO → LUMO + 2 99.6%). The calculated transitions correspond to HOMO–LUMO gaps of ΔE = 3.00 eV (**3c**)/2.88 eV (**3a**)/2.39 eV (**3b**), which reproduces the experimentally observed trend (**3c** (2.37 eV) > **3a** (2.31 eV) > **3b** (2.08 eV)). Owing to the geometry of **3b**, featuring the trigonal planar-coordinated Ni centre, DFT calculations suggest an amidinato-centred LUMO in contrast to **3a** and **3c**, where the LUMO is mostly localized at the unsubstituted Si vertices of the siliconoid ligand, resulting in a smaller HOMO–LUMO gap in **3b** (Fig. 4). The lack of spatial coincidence of HOMO and LUMO results in the smaller extinction coefficient of **3b** compared to **3a** and **3c**.

The molecular structure of **3c** in the solid state was confirmed by X-ray diffraction analysis on single crystals grown from a pentane solution at −26 °C (Fig. 5). Just as **3b**, the CO complex **3c** crystallizes in the monoclinic space group *I*2/*a*. The central geometry around the nickel centre (Si1–Ni1–Si8 108.6(4)°/C1–Ni1–C2 111.1(2)°) is like in **3a** approximately tetrahedral. The seesaw angle Si4–Si5–Si6 (173.6(5)°) is in good agreement with **3b** and the free ligand.[39,40] Ni1–Si bond distances in **3c** (Ni1–Si1 2.335(9) Å, Ni1–Si3 2.501(1) Å, Ni1–Si8 2.236(1) Å) are slightly elongated compared to **3a,b** (**3a** Ni1–Si1 2.302(5) Å, Ni1–Si3 2.428(5) Å, Ni1–Si8 2.212(5) Å; **3b** Ni1–Si1 2.216(8) Å, Ni1–Si3 2.378(8) Å, Ni1–Si8 2.183(8) Å), which can be attributed to the strong π-acceptor character of CO, leading to increased competition for metal-based backdonation and an associated weakening of the Ni–Si interaction.[22,34,64,65] The Ni1–C1/C2 (Ni1–C1 1.807(4) Å, Ni1–C2 1.799(4) Å) as well as the C–O (C1–O1 1.135(4) Å, C2–O2 1.130(5) Å) bond lengths are in the expected range.[22,34,64,65]

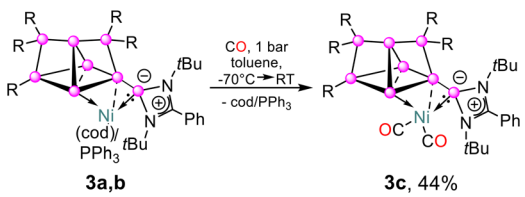

3a,b **3c**, 44%

Scheme 3 Reactivity of nickel siliconoid/silylene hybrids **3a,b** towards CO (● = Si, R = 2,4,6-triisopropylphenyl).

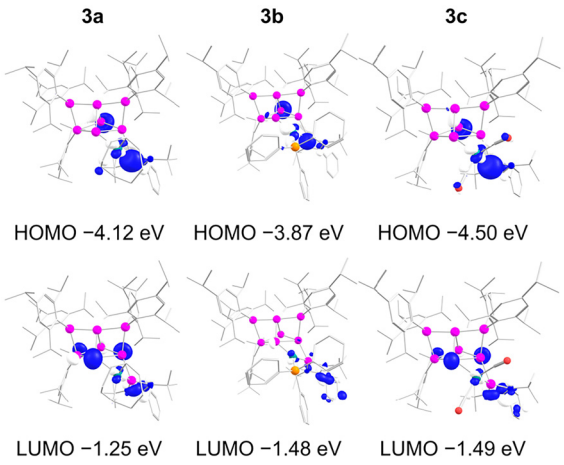

Fig. 4 Selected frontier orbitals of nickel complexes **3a–c** at the B3LYP/def2-TZVP level of theory[54–57] (contour value = 0.05).

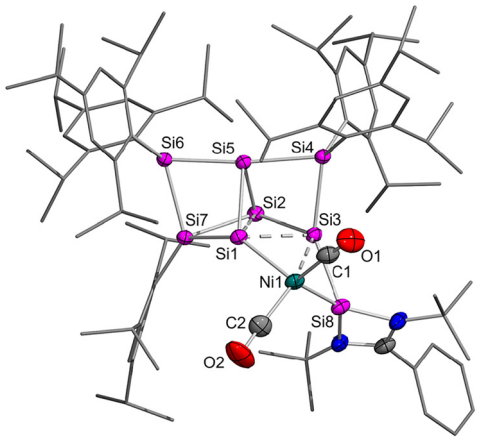

Fig. 5 Molecular structure of $Ni(CO)_2$-siliconoid/silylene complex **3c** in the solid state. Hydrogen atoms are omitted for clarity. Thermal ellipsoids at 50% probability. Selected bond lengths [Å] and angles [°]: Ni1–Si1 2.335(9), Ni1–Si3 2.501(1), Ni1–Si8 2.236(1), Ni1–C1 1.807(4), Ni1–C2 1.799(4), C1–O1 1.135(4), C2–O2 1.130(5), Si1–Si2 2.667(1), Si1–Si3 2.444(1), Si3–Si8 2.310(1); C1–Ni1–C2 111.1(2), Ni1–C1–O1 175.4(4), Ni1–C2–O2 177.3(4), Si1–Ni1–Si8 108.6(4), Si1–Si3–Ni1 56.3(3), Si8–Si3–Ni1 55.2(3), Si1–Si3–Si8 102.6(5), Si4–Si5–Si6 173.6(5).

The FT-IR spectrum of **3c** exhibits significant CO-stretching bands at 2015 and 1976 cm^{-1}. The bands in the IR spectrum of **3c** are more red-shifted in comparison with other reported Si–Ni$(CO)_n$ silylene-ligands, comparable to the NHSi–NHC–Ni$(CO)_2$ compound by Driess *et al.* ($\tilde{V}_{CO}$ = 1952 and 1887 cm^{-1}),[64] the bis(NHSi)–Ni$(CO)_2$ by Radius ($\tilde{V}_{CO}$ = 2039 and 2006 cm^{-1})[65] and the dimeric Si_9 cluster by Korber *et al.* **IX** ($\tilde{V}_{CO}$ 1999 and 1937 cm^{-1}).[34] This observation implies a similarly strong σ-donating ability of the siliconoid/silylene ligand **1** as the above mentioned low-valent silicon species, which is due to the enhanced Ni → CO π-backdonation of the electron-rich ligands.

In view of the relevance of hydrosilylation, especially in industrial scale,[66,67] precious transition metals such as platinum remain the gold standard.[68] The application of the lighter congeners, like nickel, has attracted increasing attention in recent years owing to the higher abundancy,[69–71] however most complexes only show moderate reactivity under harsh conditions.[72,73] In a preliminary test, we added a catalytic quantity of **3a** to $PhSiH_3$ to test its activity towards primary silanes. Vigorous gas evolution indicated the formation of H_2 and indeed oligo- and polysilanes are detected in the reaction mixture as major products. Apparently dehydrocoupling is the favourable reaction pathway for sterically undemanding silanes. In contrast, the tertiary silane Et_3SiH did not show any reactivity at all towards styrene in the presence of **3a**. As a compromise in terms of steric congestion, we chose the secondary silane Ph_2SiH_2, and indeed, the addition of catalytic quantities of **3a** to Ph_2SiH_2 led to the desired conversion of alkene substrates with minor formation of disilanes and higher oligomers as by-products and was therefore selected for more detailed investigations regarding the scope of alkene substrates. Reaction of cyclohexene with Ph_2SiH_2 did not show any sign for the conversion to the hydrosilylation product even after 72 h, instead exhibiting signals assigned to the formation of tetraphenyldisilane and the according hydrogenation product cyclohexane. We concluded that the steric hindrance is limiting the accessibility of the catalyst and hence, only the de-hydrocoupling side-reaction followed by hydrogenation is observed in case of internal alkenes (see NMR spectra in the SI), and we thus turned our attention to terminal alkenes.

To identify optimal reaction conditions, we performed a more detailed pre-screening for the hydrosilylation of vinyltrimethylsilane with Ph_2SiH_2 in the presence of variable catalyst loadings of **3a–c** (Table 2). With 0.5 mol% of catalyst **3a** in C_6D_6 at ambient temperatures, we observed full conversion of vinyltrimethylsilane after two hours under formation of the anti-Markovnikov product **A** in 46% spectroscopic yield (entry

Table 2 Screening of the reaction conditions for the hydrosilylation catalysis of vinyltrimethylsilane (mesitylene as internal standard)

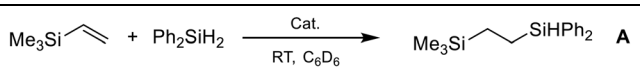

Entry	Cat.	Cat. loading [mol%]	Conversion [%]	Spectr. yield **A** [%]	Time [h]
1	None	0	0	0	>48
2	**3a**	0.5	>99	46	2[a]
3	**3a**	0.05	>99	45	8
4	**3a**	0.05	>99	23	72[b]
5	**3b**	0.5	29	24	48[a]
6	**3b**	0.05	8	0	48
7	**3c**	0.5	8	0	48[a]
8	**3c**	0.05	4	0	48
9	Ni $(cod)_2$	0.5	>99	43	<1
10	Ni $(cod)_2$	0.05	>99	42	5.5
11	Ni $(cod)_2$	0.05	>99	31	5.5[b]

[a] 0.6 mmol substrate, 1.1 eq. diphenylsilane. [b] In the presence of Hg.

2). Lowering the catalyst loading to 0.05 mol%, required a longer reaction time of 8 h (**A** 45%, entry 3), yet the selectivity for **A** over by-products such as oligosilanes and presumably the twofold-substituted silylation product remains virtually unaffected. There are no indications for the formation of the Markovnikov product **M** in these cases. A mercury drop test revealed a slower reaction to **A** with an overall lower spectroscopic yield, however exhibiting a higher ratio of **A** compared to the twofold-substituted silylation product (23 : 6) than in the reaction without the presence of Hg (9 : 5).(entry 4), indicating that the catalyst is partially decomposed to nickel particles in the course of the reaction, which are known to be highly active but unselective in heterogenous catalysis.[74,75] A blank run without any catalyst gave no conversion at all after more than 48 h (entry 1). Employing phosphine and carbonyl derivatives **3b** and **3c** as catalysts resulted in incomplete conversions at 0.5 mol% and a negligible conversion at 0.05% (entries 5 to 7). Their lack of catalytic activity can be attributed to the tighter coordination of the phosphine and carbonyl ligands in **3b** and **3c** compared to the cod ligand in **3a**, blocking the binding site for the alkene and silane substrates more effectively. Intended as another control experiment with regard to the precatalytic activity, we probed the catalysis with 0.5 mol% of $Ni(cod)_2$ under the same conditions as for **3a**. Surprisingly, an even faster conversion of vinyltrimethylsilane (50 minutes, entry 9) was observed. With reduced catalyst loading 0.05 mol% of $Ni(cod)_2$ full conversion is achieved after 5.5 h, with the anti-Markovnikov species **A** as the major product (42.5%, entry 10). Although there are many examples reported for the hydrosilylation with $Ni(cod)_2$ in combination with a stabilizing ligand, *e.g.* phosphines or NHCs,[76,77] there are only very few reports on catalysis using $Ni(cod)_2$ itself on substrates such as styrene,[78] α-(trifluormethyl)styrene[79] and imines.[80] To the best of our knowledge, the $Ni(cod)_2$-catalysed hydrosilylation of unactivated terminal alkenes has never been reported. While **3a** is thus somewhat less active than $Ni(cod)_2$ itself, it can still be considered a competent catalyst for the anti-Markovnikov hydrosilylation of vinyltrimethylsilane.

After the preliminary optimization of the reaction parameters with the vinyltrimethylsilane benchmark, we sought to expand the substrate scope to other terminal alkenes. Additional electron-rich examples, namely 1-hexene, vinyl- and allyl cyclohexane, and allyltrimethylsilane were investigated but also comparatively electron-poor styrene and allylbenzene included for comparison. Reactions were carried out at ambient temperature in C_6D_6 with the catalyst load kept constant at 0.05 mol% of **3a** (Table 3). As above, control experiments employing $Ni(cod)_2$ as the catalyst were performed under the same conditions for comparison (see SI, Table S1). While the anti-Markovnikov product **A** is obtained without any sign for the formation of the Markovnikov product **M** in the electron rich cases (entries 1 to 5), electron-poor styrene and allylbenzene unexpectedly gave rise to the branched product in an almost 1 : 1 ratio (entries 6 and 7).[68,81–83] Note that Markovnikov hydrosilylation – formerly considered an undesired outcome – has been moving into focus in recent years.[67]

Concerning the hydrosilylation with catalyst **3a**, a general trend becomes apparent. While all cases investigated react to full conversion resulting in turn-over numbers (TONs) of approximately 2000, higher turnover frequencies (TOFs) up to

Table 3 Catalytic hydrosilylation of terminal olefins with Ph_2SiH_2 using nickel complex **3a** as a homogeneous catalyst

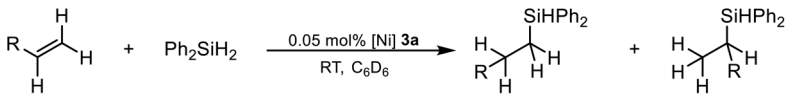

Entry	Substrate	Time [h]	Conversion [%]	Product	Spectr. yield [%]	TOF [h^{-1}]
1		0.25	>99	**A**	39	8000
2A	Me_3Si	1	30	**A**	24	640
2B		4	79	**A**	40	400
2C		8	>99	**A**	45	250
3A	Me_3Si	8	27	**A**	20	67
3B		192	83	**A**	45	9
3C		408	>99	**A**	48	5
4A		0.08	60	**A**	33	14 300
4B		72	97	**A**	37	27
4C		168	>99	**A**	59	12
5A		0.5	34	**A**	13	1350
5B		192	85	**A**	38	9
5C		408	>99	**A**	40	5
6A		2	33	**A : M**	9 : 16	530
6B		24	90	**A : M**	23 : 29	75
6C		54	>99	**A : M**	27 : 31	37
7A		0.5	30	**A : M**	18 : 13	1190
7B		24	88	**A : M**	33 : 32	73
7C		54	>99	**A : M**	38 : 34	37

8000 h^{-1} are observed for the open chain substrates such as 1-hexene (entry 1) and the vinyl-substituted alkenes (entries 2, 4 and 6). Spectroscopic yields of **A** up to 59% (entries 1, 2C and 4C) are obtained without any evidence for the formation of the Markovnikov product (**M**). On the other hand, the allyl-substituted substrates (entries 3 and 5) show rather slow conversions with TOFs down to 5 h^{-1} and spectroscopic yields of **A** around 40–48% (entry 3C and 5C). In contrast, the electron-poor substrates styrene and allylbenzene (entry 6 and 7) produce an almost equimolar spectroscopic ratio of **M** to **A** with TOFs of around 37 h^{-1} at full conversion. Presumably due to catalyst degradation, the TOFs are decreasing during the progress of the reactions (entries 2–7 A *vs.* B *vs.* C). Moreover, the formation of unidentifiable/volatile byproducts reduces the (spectroscopic) yield of the **A**/**M** hydrosilylation products.

To put the obtained results into perspective: Tilley *et al.* reported a dimeric, halogenated Ni catalyst reaching TONs of up to 970 (0.1 mol%, 17 h at 23 °C) with a selectivity ratio of 3 : 1 in favour of terminal hydrosilylation,[84] while a nickel pincer complex reported by the group of Hu on the other hand, gives even higher TONs and TOFs (up to 100 000 h^{-1} at 0.01 mol%/83 000 h^{-1} at 0.025 mol%).[85] Employing $Ni(cod)_2$ as the catalyst results in instant conversion of 1-hexene reiterating the result with vinyltrimethylsilane as a substrate (see SI, Table S1). Allylcyclohexane and allyltrimethylsilane were not fully converted in the presence of $Ni(cod)_2$ even after 21 days likely because of catalyst degradation (see SI, Table S1). In contrast, **3a** resulted in full conversion of both substrates, albeit slowly (TOF 5 h^{-1} each, entries 3C and 5C, Table 3).

Conclusions

In summary, we reported the preparation and full characterization of a terminal $Fe(CO)_4$ complex of a Si_7/silylene hybrid ligand. Unlike in the case of the corresponding Si_6/silylene system, the lower steric demand of the organic residues per silicon cluster vertex also allowed for the preparation of a series of the first stable nickel complexes of a siliconoid/silylene with 1,5-cyclooctadiene, triphenylphosphine and carbon monoxide acting as auxiliary ligands. The coordination environment of the PPh_3 derivative stands out with a trigonal planar nickel centre while the cod and CO complexes show distorted tetrahedral nickel coordination spheres. The cod-coordinated nickel complex turned out to be active in the hydrosilylation of terminal alkenes with an interesting preference for anti-Markovnikov regioselectivity in case of electron-richer substrates and unselective formation of both regiomers for electron-poor alkenes.

Author contributions

L. Giarrana performed the synthetic work and data analysis with partial support by D. Welterlich; L. Giarrana. and D. Scheschkewitz designed the study. D. Scheschkewitz acquired the funding; B. Morgenstern performed the X-ray diffraction studies. M. Zimmer performed the solid state and variable temperature NMR measurements. L. Giarrana performed the DFT calculations. L. Giarrana wrote the initial manuscript draft. L. Giarrana and D. Scheschkewitz reviewed and edited the manuscript.

Conflicts of interest

There are no conflicts of interest to declare.

Data availability

All data associated with this manuscript are available in the supplementary information (SI). Supplementary information is available. See DOI: **https://doi.org/10.1039/d6qi00025h**.

CCDC 2504459 (**2**), 2504461 (**3a**), 2504467 (**3b**) and 2504470 (**3c**) contain the supplementary crystallographic data for this paper.[86a–d]

Acknowledgements

Funding by the Deutsche Forschungsgemeinschaft (DFG SCHE 906/4-4) is gratefully acknowledged. Instrumentation and technical assistance for this work were provided by the Service Center X-ray Diffraction, with financial support from Saarland University and German Science Foundation (project number INST 256/506-1). The authors thank Prof. Stella Stopkowicz for access to her computational cluster.

References

1 R. H. Crabtree, *The Organometallic Chemistry of the Transition Metals*, John Wiley & Sons, Hoboken, NJ, 2009.
2 K. S. Egorova and V. P. Ananikov, Which metals are green for catalysis? Comparison of the toxicities of Ni, Cu, Fe, Pd, Pt, Rh, and Au salts, *Angew. Chem., Int. Ed.*, 2016, **55**, 12150.
3 T. J. Hadlington, Heavier tetrylene-and tetrylyne-transition metal chemistry: it's no carbon copy, *Chem. Soc. Rev.*, 2024, **53**, 9738.
4 W. I. Dzik, X. P. Zhang and B. de Bruin, Redox noninnocence of carbene ligands: carbene radicals in (catalytic) C–C bond formation, *Inorg. Chem.*, 2011, **50**, 9896.
5 K.-S. Feichtner and V. H. Gessner, Cooperative bond activation reactions with carbene complexes, *Chem. Commun.*, 2018, **54**, 6540.
6 R. C. Cammarota, L. J. Clouston and C. C. Lu, Leveraging molecular metal–support interactions for H_2 and N_2 activation, *Chem. Rev.*, 2017, **334**, 100.
7 R. C. Cammarota, J. Xie, S. A. Burgess, M. V. Vollmer, K. D. Vogiatzis, J. Ye, J. C. Linehan, A. M. Appel, C. Hoffmann, X. Wang, V. G. Young and C. C. Lu,

Thermodynamic and kinetic studies of H_2 and N_2 binding to bimetallic nickel-group 13 complexes and neutron structure of a Ni(η^2-H_2) adduct, *Chem. Sci.*, 2019, **10**, 7029.

8 M. J. Dorantes, J. T. Moore, E. Bill, B. Mienert and C. C. Lu, Bimetallic iron–tin catalyst for N_2 to NH_3 and a silyldiazenido model intermediate, *Chem. Commun.*, 2020, **56**, 11030.

9 B. J. Graziano, M. V. Vollmer and C. C. Lu, Cooperative bond activation and facile intramolecular aryl transfer of nickel–aluminum pincer–type complexes, *Angew. Chem., Int. Ed.*, 2021, **60**, 15087.

10 J. T. Moore, M. J. Dorantes, Z. Pengmei, T. M. Schwartz, J. Schaffner, S. L. Apps, C. A. Gaggioli, U. Das, L. Gagliardi, D. A. Blank and C. C. Lu, Light–Driven Hydrodefluorination of Electron–Rich Aryl Fluorides by an Anionic Rhodium–Gallium Photoredox Catalyst, *Angew. Chem., Int. Ed.*, 2022, **61**, e202205575.

11 B. Blom, D. Gallego and M. Driess, N-heterocyclic silylene complexes in catalysis: new frontiers in an emerging field, *Inorg. Chem. Front.*, 2014, **1**, 134.

12 R. Waterman, P. G. Hayes and T. D. Tilley, Synthetic development and chemical reactivity of transition-metal silylene complexes, *Acc. Chem. Res.*, 2007, **40**, 712.

13 A. V. Protchenko, J. I. Bates, L. M. A. Saleh, M. P. Blake, A. D. Schwarz, E. L. Kolychev, A. L. Thompson, C. Jones, P. Mountford and S. Aldridge, Enabling and probing oxidative addition and reductive elimination at a group 14 metal center: cleavage and functionalization of E–H bonds by a bis (boryl) stannylene, *J. Am. Chem. Soc.*, 2016, **138**, 4555.

14 T. J. Hadlington, J. A. B. Abdalla, R. Tirfoin, S. Aldridge and C. Jones, Stabilization of a two-coordinate, acyclic diaminosilylene (ADASi): completion of the series of isolable diaminotetrylenes: E (NR 2) 2 (E= group 14 element), *Chem. Commun.*, 2016, **52**, 1717.

15 D. C. H. Do, A. V. Protchenko, M.Á Fuentes, J. Hicks, P. Vasko and S. Aldridge, N–H cleavage vs. Werner complex formation: reactivity of cationic group 14 tetrelenes towards amines, *Chem. Commun.*, 2020, **56**, 4684.

16 Z. Mo, T. Szilvási, Y. Zhou, S. Yao and M. Driess, An Intramolecular Silylene Borane Capable of Facile Activation of Small Molecules, Including Metal–Free Dehydrogenation of Water, *Angew. Chem., Int. Ed.*, 2017, **56**, 3699.

17 D. Wendel, A. Porzelt, F. A. D. Herz, D. Sarkar, C. Jandl, S. Inoue and B. Rieger, From Si(II) to Si(IV) and back: reversible intramolecular carbon–carbon bond activation by an acyclic iminosilylene, *J. Am. Chem. Soc.*, 2017, **139**, 8134.

18 S. Takahashi, E. Bellan, A. Baceiredo, N. Saffon-Merceron, S. Massou, N. Nakata, D. Hashizume, V. Branchadell and T. Kato, A Stable N–Hetero–*Rh*–Metallacyclic Silylene, *Angew. Chem., Int. Ed.*, 2019, **58**, 10310.

19 A. Meltzer, C. Präsang and M. Driess, Diketiminate silicon (II) and related NHSi ligands generated in the coordination sphere of nickel (0), *J. Am. Chem. Soc.*, 2009, **131**, 7232.

20 S. Z. Tasker, E. A. Standley and T. F. Jamison, Recent advances in homogeneous nickel catalysis, *Nature*, 2014, **509**, 299.

21 V. Vermaak, H. C. M. Vosloo and A. J. Swarts, The development and application of homogeneous nickel catalysts for transfer hydrogenation and related reactions, *Coord. Chem. Rev.*, 2024, **507**, 215716.

22 G. Tavčar, S. S. Sen, R. Azhakar, A. Thorn and H. W. Roesky, Facile syntheses of silylene nickel carbonyl complexes from Lewis base stabilized chlorosilylenes, *Inorg. Chem.*, 2010, **49**, 10199.

23 C. Watanabe, Y. Inagawa, T. Iwamoto and M. Kira, Synthesis and structures of (dialkylsilylene) bis (phosphine)-nickel, palladium, and platinum complexes and (η^6-arene)(dialkylsilylene) nickel complexes, *Dalton Trans.*, 2010, **39**, 9414.

24 T. J. Hadlington, T. Szilvási and M. Driess, Silylene–Nickel Promoted Cleavage of B–O Bonds: From Catechol Borane to the Hydroborylene Ligand, *Angew. Chem., Int. Ed.*, 2017, **56**, 7470.

25 N. C. Breit, T. Szilvási, T. Suzuki, D. Gallego and S. Inoue, From a zwitterionic phosphasilene to base stabilized silyliumylidene-phosphide and bis (silylene) complexes, *J. Am. Chem. Soc.*, 2013, **135**, 17958.

26 Y. Wang, A. Kostenko, S. Yao and M. Driess, Divalent silicon-assisted activation of dihydrogen in a bis (N-heterocyclic silylene) xanthene nickel (0) complex for efficient catalytic hydrogenation of olefins, *J. Am. Chem. Soc.*, 2017, **139**, 13499.

27 Y. Zhou, S. Raoufmoghaddam, T. Szilvási and M. Driess, A Bis(silylene)–Substituted *ortho*–Carborane as a Superior Ligand in the Nickel–Catalyzed Amination of Arenes, *Angew. Chem., Int. Ed.*, 2016, **55**, 12868.

28 W. Yang, Y. Dong, H. Sun and X. Li, Progress in the preparation and characterization of silylene iron, cobalt and nickel complexes, *Dalton Trans.*, 2021, **50**, 6766.

29 Y. Heider and D. Scheschkewitz, Stable unsaturated silicon clusters (siliconoids), *Dalton Trans.*, 2018, **47**, 7104.

30 Y. Heider and D. Scheschkewitz, Molecular silicon clusters, *Chem. Rev.*, 2021, **121**, 9674.

31 Y. Wang, J. E. McGrady and Z.-M. Sun, Solution-Based Group 14 Zintl Anions: New Frontiers and Discoveries, *Acc. Chem. Res.*, 2021, **54**, 1506.

32 J. M. Goicoechea and S. C. Sevov, Deltahedral germanium clusters: insertion of transition-metal atoms and addition of organometallic fragments, *J. Am. Chem. Soc.*, 2006, **128**, 4155.

33 O. P. E. Townrow, C. Chung, S. A. Macgregor, A. S. Weller and J. M. Goicoechea, A neutral heteroatomic zintl cluster for the catalytic hydrogenation of cyclic alkenes, *J. Am. Chem. Soc.*, 2020, **142**, 18330.

34 S. Joseph, M. Hamberger, F. Mutzbauer, O. Härtl, M. Meier and N. Korber, Chemistry with Bare Silicon Clusters in Solution: A Transition–Metal Complex of a Polysilicide Anion, *Angew. Chem., Int. Ed.*, 2009, **48**, 8770.

35 L. J. Schiegerl, A. J. Karttunen, W. Klein and T. F. Fässler, Anionic Siliconoids from Zintl Phases: $R_3Si_9^-$ with Six and $R_2Si_9^{2-}$ with Seven Unsubstituted Exposed Silicon Cluster Atoms (R=Si(tBu)$_2$H), *Chem. – Eur. J.*, 2018, **24**, 19171.

36 N. E. Poitiers, L. Giarrana, K. I. Leszczyńska, V. Huch, M. Zimmer and D. Scheschkewitz, Indirect and Direct Grafting of Transition Metals to Siliconoids, *Angew. Chem., Int. Ed.*, 2020, **59**, 8532.
37 N. E. Poitiers, L. Giarrana, V. Huch, M. Zimmer and D. Scheschkewitz, Exohedral functionalization vs. core expansion of siliconoids with Group 9 metals: catalytic activity in alkene isomerization, *Chem. Sci.*, 2020, **11**, 7782.
38 N. E. Poitiers, V. Huch, M. Zimmer and D. Scheschkewitz, Nickel-assisted complete cleavage of CO by a silylene/siliconoid hybrid under formation of an Si=C enol ether bridge, *Chem. Commun.*, 2020, **56**, 10898.
39 K. I. Leszczyńska, V. Huch, C. Präsang, J. Schwabedissen, R. J. F. Berger and D. Scheschkewitz, Atomically precise expansion of unsaturated silicon clusters, *Angew. Chem., Int. Ed.*, 2019, **58**, 5124.
40 L. Giarrana, M. Zimmer, B. Morgenstern and D. Scheschkewitz, Tetrylene-Functionalized Si_7−Siliconoids, *Inorg. Chem.*, 2024, **63**, 20083.
41 W. Yang, H. Fu, H. Wang, M. Chen, Y. Ding, H. W. Roesky and A. Jana, A base-stabilized silylene with a tricoordinate silicon atom as a ligand for a metal complex, *Inorg. Chem.*, 2009, **48**, 5058.
42 T. A. Schmedake, M. Haaf, B. J. Paradise, A. J. Millevolte, D. R. Powell and R. West, Electronic and steric properties of stable silylene ligands in metal (0) carbonyl complexes, *J. Organomet. Chem.*, 2001, **636**, 17.
43 N. C. Breit, C. Eisenhut and S. Inoue, Phosphinosilylenes as a novel ligand system for heterobimetallic complexes, *Chem. Commun.*, 2016, **52**, 5523.
44 F. H. Carre and J. J. E. Moreau, Reactivity of μ-Silanediyl Iron Carbonyl Complexes with Alkynes. Molecular Structure of $(CO)_4FeSiPh_2CEt{=}CEtSiPh_2$ and of $(CO)_3FeCMe{=}CMeSiPh_2CMe{=}CMeFe(CO)_3$, *Inorg. Chem.*, 1982, **21**, 3099.
45 R. Dorta, E. D. Stevens, N. M. Scott, C. Costabile, L. Cavallo, C. D. Hoff and S. P. Nolan, Steric and Electronic Properties of N-Heterocyclic Carbenes (NHC): A Detailed Study on Their Interaction with $Ni(CO)_4$, *J. Am. Chem. Soc.*, 2005, **127**, 2485.
46 H. Clavier and S. P. Nolan, Percent buried volume for phosphine and N-heterocyclic carbene ligands: steric properties in organometallic chemistry, *Chem. Commun.*, 2010, **46**, 841.
47 L. Falivene, Z. Cao, A. Petta, L. Serra, A. Poater, R. Oliva, V. Scarano and L. Cavallo, Towards the online computer-aided design of catalytic pockets, *Nat. Chem.*, 2019, **11**, 872.
48 L. Falivene, R. Credendino, A. Poater, A. Petta, L. Serra, R. Oliva, V. Scarano and L. Cavallo, SambVca 2. A web tool for analyzing catalytic pockets with topographic steric maps, *Organometallics*, 2016, **35**, 2286.
49 A. Hinz, Pseudo–one–coordinate tetrylenium salts bearing a bulky carbazolyl substituent, *Chem. – Eur. J.*, 2019, **25**, 3267.
50 T. George, T. Grant, I. S. Munhoz, T. Do and J. D. Masuda, Group 11 complexes of a bulky triazene ligand, *Dalton Trans.*, 2024, **53**, 13107.
51 M. Alkan-Zambada, E. C. Constable and C. E. Housecroft, The role of percent volume buried in the characterization of copper(I) complexes for lighting purposes, *Molecules*, 2020, **25**, 2647.
52 D. Lutters, C. Severin, M. Schmidtmann and T. Müller, Activation of 7-silanorbornadienes by N-heterocyclic carbenes: a selective way to N-heterocyclic-carbene-stabilized silylenes, *J. Am. Chem. Soc.*, 2016, **138**, 6061.
53 R. S. Berry, Correlation of rates of intramolecular tunneling processes, with application to some group V compounds, *J. Chem. Phys.*, 1960, **32**, 933.
54 A. D. Becke, Density–functional thermochemistry. III. The role of exact exchange, *J. Chem. Phys.*, 1993, **98**, 5648.
55 C. Lee, W. Yang and R. G. Parr, Development of the Colle-Salvetti correlation-energy formula into a functional of the electron density, *Phys. Rev. B:Condens. Matter Mater. Phys.*, 1988, **37**, 785.
56 F. Weigend and R. Ahlrichs, Balanced basis sets of split valence, triple zeta valence and quadruple zeta valence quality for H to Rn: Design and assessment of accuracy, *Phys. Chem. Chem. Phys.*, 2005, **7**, 3297.
57 F. Weigend, Accurate Coulomb-fitting basis sets for H to Rn, *Phys. Chem. Chem. Phys.*, 2006, **8**, 1057.
58 W. Wang, S. Inoue, S. Yao and M. Driess, An isolable bis-silylene oxide ("disilylenoxane") and its metal coordination, *J. Am. Chem. Soc.*, 2010, **132**, 15890.
59 M. Haaf, T. A. Schmedake and R. West, Stable silylenes, *Acc. Chem. Res.*, 2000, **33**, 704.
60 M.-P. Lücke, S. Yao and M. Driess, Boosting homogeneous chemoselective hydrogenation of olefins mediated by a bis (silylenyl) terphenyl-nickel (0) pre-catalyst, *Chem. Sci.*, 2021, **12**, 2909.
61 M. Stoelzel, C. Präsang, S. Inoue, S. Enthaler and M. Driess, Hydrosilylation of Alkynes by Ni $(CO)_3$−Stabilized Silicon(II) Hydride, *Angew. Chem., Int. Ed.*, 2012, **51**, 399.
62 S. Grimme, A. Hansen, J. G. Brandenburg and C. Bannwarth, Dispersion-corrected mean-field electronic structure methods, *Chem. Rev.*, 2016, **116**, 5105.
63 V. N. Staroverov, G. E. Scuseria, J. Tao and J. P. Perdew, Comparative assessment of a new nonempirical density functional: Molecules and hydrogen-bonded complexes, *J. Chem. Phys.*, 2003, **119**, 12129.
64 G. Tan, S. Enthaler, S. Inoue, B. Blom and M. Driess, Synthesis of Mixed Silylene–Carbene Chelate Ligands from N–Heterocyclic Silylcarbenes Mediated by Nickel, *Angew. Chem., Int. Ed.*, 2015, **54**, 2214.
65 E. Glok, L. Werner and U. Radius, N-Heterocyclic silylene complexes of nickel (0), *Dalton Trans.*, 2025, **54**, 14846.
66 D. Troegel and J. Stohrer, Recent advances and actual challenges in late transition metal catalyzed hydrosilylation of olefins from an industrial point of view, *Coord. Chem. Rev.*, 2011, **255**, 1440.
67 M. Zaranek and P. Pawluc, Markovnikov hydrosilylation of alkenes: how an oddity becomes the goal, *ACS Catal.*, 2018, **8**, 9865.

68 L. D. de Almeida, H. Wang, K. Junge, X. Cui and M. Beller, Recent advances in catalytic hydrosilylations: developments beyond traditional platinum catalysts, *Angew. Chem., Int. Ed.*, 2021, **60**, 550.
69 Y. Nakajima, K. Sato and S. Shimada, Development of nickel hydrosilylation catalysts, *Chem. Rec.*, 2016, **16**, 2379.
70 X. Wu, G. Ding, W. Lu, L. Yang, J. Wang, Y. Zhang, X. Xie and Z. Zhang, Nickel-catalyzed hydrosilylation of terminal alkenes with primary silanes via electrophilic silicon–hydrogen bond activation, *Org. Lett.*, 2021, **23**, 1434.
71 I. Pappas, S. Treacy and P. J. Chirik, Alkene Hydrosilylation Using Tertiary Silanes with α-Diimine Nickel Catalysts. Redox-Active Ligands Promote a Distinct Mechanistic Pathway from Platinum Catalysts, *ACS Catal.*, 2016, **6**, 4105.
72 X. Du and Z. Huang, Advances in base-metal-catalyzed alkene hydrosilylation, *ACS Catal.*, 2017, **7**, 1227.
73 H. Maciejewski, B. Marciniec and I. Kownacki, Catalysis of hydrosilylation: Part XXXIV. High catalytic efficiency of the nickel equivalent of Karstedt catalyst [{Ni(η-CH_2=CHSiMe_2)$_2$O}$_2${μ-(η-CH_2=CHSiMe_2)$_2$O}], *J. Organomet. Chem.*, 2000, **597**, 175.
74 V. M. Chernyshev, A. V. Astakhov, I. E. Chikunov, R. V. Tyurin, D. B. Eremin, G. S. Ranny, V. N. Khrustalev and V. P. Ananikov, Pd and Pt catalyst poisoning in the study of reaction mechanisms: what does the mercury test mean for catalysis?, *ACS Catal.*, 2019, **9**, 2984.
75 I. C. Chagunda, T. Fisher, M. Schierling and J. S. McIndoe, Poisonous Truth about the Mercury Drop Test: The Effect of Elemental Mercury on Pd (0) and Pd(II) ArX Intermediates, *Organometallics*, 2023, **42**, 2938.
76 A. S. Chang, K. E. Kawamura, H. S. Henness, V. M. Salpino, J. C. Greene, L. N. Zakharov and A. K. Cook, (NHC) Ni (0)-catalyzed branched-selective alkene hydrosilylation with secondary and tertiary silanes, *ACS Catal.*, 2022, **12**, 11002.
77 Z. D. Miller, W. Li, T. R. Belderrain and J. Montgomery, Regioselective Allene Hydrosilylation Catalyzed by *N*-Heterocyclic Carbene Complexes of Nickel and Palladium, *J. Am. Chem. Soc.*, 2013, **135**, 15282.
78 B. Marciniec, H. Maciejewski and I. Kownacki, Dehydrogenative coupling of styrene with trisubstituted silanes catalyzed by nickel complexes, *J. Mol. Catal. A: Chem.*, 1998, **135**, 223.
79 D. Bai, K. Zhong, L. Chang, Y. Qiao, F. Wu, G. Xu and J. Chang, Nickel-catalyzed regiodivergent hydrosilylation of α-(fluoroalkyl) styrenes without defluorination, *Nat. Commun.*, 2024, **15**, 6360.
80 D. P. Spence, *Hydrosilylation of Imines Using a Ni (0) Catalyst*, Master Thesis, UC San Diego, 2016.
81 Y. Wei, S.-X. Liu, H. Mueller-Bunz and M. Albrecht, Synthesis of triazolylidene nickel complexes and their catalytic application in selective aldehyde hydrosilylation, *ACS Catal.*, 2016, **6**, 8192.
82 I. Buslov, S. C. Keller and X. Hu, Alkoxy hydrosilanes as surrogates of gaseous silanes for hydrosilylation of alkenes, *Org. Lett.*, 2016, **18**, 1928.
83 Y. Chen, C. Sui-Seng, S. Boucher and D. Zargarian, Influence of $SiMe_3$ Substituents on Structures and Hydrosilylation Activities of ((SiMe_3)$_{1\ or\ 2}$-Indenyl)Ni(PPh_3)Cl, *Organometallics*, 2005, **24**, 149.
84 J. Yang, V. Postils, M. I. Lipschutz, M. Fasulo, C. Raynaud, E. Clot, O. Eisenstein and T. D. Tilley, Efficient alkene hydrosilation with bis (8-quinolyl) phosphine (NPN) nickel catalysts. The dominant role of silyl-over hydrido-nickel catalytic intermediates, *Chem. Sci.*, 2020, **11**, 5043.
85 I. Buslov, J. Becouse, S. Mazza, M. Montandon-Clerc and X. Hu, Chemoselective alkene hydrosilylation catalyzed by nickel pincer complexes, *Angew. Chem., Int. Ed.*, 2015, **54**, 14523.
86 (*a*) CCDC 2504459: Experimental Crystal Structure Determination, 2026, DOI: **10.5517/ccdc.csd.cc2q230y**; (*b*) CCDC 2504461: Experimental Crystal Structure Determination, 2026, DOI: **10.5517/ccdc.csd.cc2q2320**; (*c*) CCDC 2504467: Experimental Crystal Structure Determination, 2026, DOI: **10.5517/ccdc.csd.cc2q2386**; (*d*) CCDC 2504470: Experimental Crystal Structure Determination, 2026, DOI: **10.5517/ccdc.csd.cc2q23c9**.